Scaling of density peaking in JET H-modes

H. Weisen[1], A. Zabolotsky[1], M. Maslov[1], C. Giroud[2], and JET EFDA contributors*

email: henri.weisen@epfl.ch

[1)]Centre de Recherches en Physique des Plasmas,
Association EURATOM - Confédération Suisse, EPFL, 1015 Lausanne, Switzerland
[2)]UKAEA, Abingdon, UK

Abstract: Results from an extensive profile database analysis of JET density profiles in H-mode, show that the density peaking factor $n_{e0}/\langle n_e\rangle$ in JET H-modes increases as the effective collisionality $\nu_{eff}\approx 10^{-14} R Z_{eff} n_e/T_e^2$ drops from ~1 to the low values expected for ITER (~0.06 for the inductive reference scenario). Density peaking is also correlated with Greenwald number N_G, particle outward flux Γ from the neutral beam source and T_i/T_e. The influence of parameters related to magnetic shear, such as l_i and q_{95} is weak and ambiguous. There is no significant correlation with β_N, ρ^*, L_{Te} and L_{Ti}. Scaling expressions developed using many combinations of parameters show that ν_{eff} is the most important scaling parameter. H-modes heated only by ICRH are on average only slightly less peaked than H-modes dominated by NBI, demonstrating that neutral beam fuelling can only explain a modest part (~20%) of the peaking. Scaling expressions involving ν_{eff}, N_G, $RG/(n_e\chi)$ and T_i/T_e suggest that $n_{e0}/\langle n_e\rangle$ may exceed 1.5 in ITER, providing a boost of fusion power of more than 30% for fixed β and N_G with respect to the usual assumption of a flat density profile.

1. Introduction

The very existence of anomalous pinches leading to peaked density profiles has been established unambigously in fully radiofrequency-current driven L-mode discharges in Tore Supra [1] and TCV [2]. The view that density peaking in H-modes may also be a consequence of anomalous inward pinches has however regularly been questioned, on the basis that H-mode plasmas in the existing experimental database have a finite inductive field and are neutral beam fuelled[3][4][5]. Even the penetration of edge neutrals has been considered as a possible contributor to density peaking [5]. In this paper we show that neither of these mechanisms is sufficient to explain the existence of peaked density profiles in JET H-modes, making the conclusion of the anomalous nature of density peaking in H-modes unescapable. We then proceed to search for scalings of the peakedness of the density profiles suitable for extrapolations to ITER. The instrument of this investigation is a profile database of a wide variety of H-modes in JET, which

contains equilibrium profiles from EFIT reconstructions, particle and power deposition profiles allowing steady state heat and particle balances to be computed for each of the 300 time-slice samples in the database. Table 1 shows the range of variation of the most important number of dimensional and dimensionless parameters. Both conventional H-modes and 'hybrid', characterised by a wide core region with flat shear are represented in the database.

Table1: Range of parameters

	IP MA	BT T	$\bar{n}_{e19}$	P_{NBI} MW	P_{IC} MW	P_{LH} MW	ν_{*ei}	ν_{eff}	ρ^*	β_T	β_N	T_i/T_e	q_{95}	l_i	N_G
min	0.9	0.8	1.7	0	0	0	0.01	0.05	0.02	0.44	0.5	1.8	2.25	0.68	0.2
max	3.7	3.7	10	18	12	3	0.4	2	0.01	3.9	3.3	0.5	6.4	1.1	1

2. Conventional terms in the particle balance

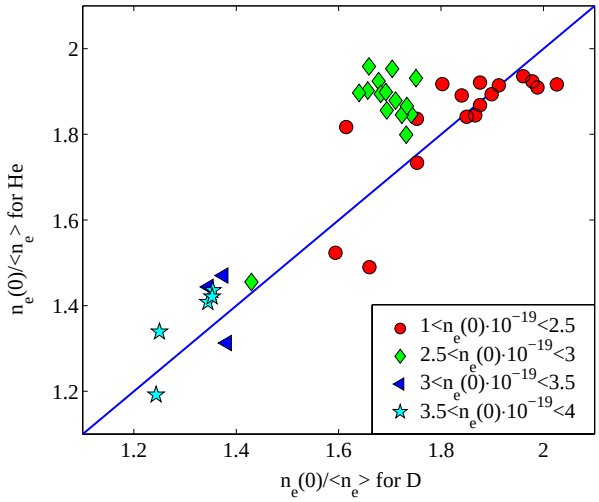

Fig. 1 Comparison of peaking factors in deuterium plasmas and in helium plasmas.

The effect of edge neutrals has been shown to be too weak to contribute to sustaining density gradients, based on neutral penetration calculations and on experimental evidence from a comparison of deuterium and He discharges [6]. Since the cross section for double CX in He is one order of magnitude smaller than that for CX in deuterium, the CX chains, which provide the mechanism for inward neutral transport, are effectively quenched in He^{++} plasmas. Despite such a fundamental difference, density profiles in He plasmas are no less peaked than their identical D^+ counterparts (fig.1), produced in two dedicated experimental campaigns, ruling out any influence of edge neutral on core density gradients.

The majority of H-mode plasmas in JET are dominated by NBI heating and therefore have a core source of particles, which may be expected to contribute to sustaining density gradients. The contribution of beam fuelling to the density gradients in steady state may be estimated as $\nabla n_e/n_e)_{NBI}=\Gamma_{NBI}/(Dn_e)$. For a typical JET plasma with $n_e\sim5\times10^{19}m^{-3}$ and 10 MW of NBI heating, the fuelling rate is some $10^{21}s^{-1}$, of which some 40% are deposited inside r/a=0.5, corresponding to $\Gamma_{NBI}\sim5\times10^{18}m^{-2}s^{-1}$. Hence, in order to sustain a typical gradient

$|\nabla n_e|/n_e \sim 1m^{-1}$, D would have to be of order $0.1m^2/s$, a low value when compared to heat diffusivity. Unlike heat diffusivities, particle diffusivities cannot be obtained on a routine basis. We therefore relate the beam fuelling contribution to the effective heat diffusivity $\chi=Q/(n_e\nabla T_e+n_i\nabla T_i)\approx Q/(2n_e\nabla T_e)$, where Q is the total heat flux, as follows:

$$\left.\frac{\nabla n_e}{n_e}\right)_{NBI} = \frac{\Gamma_{NBI}}{Dn_e} \approx \frac{\chi}{D}\cdot\frac{T_e}{Q/\Gamma_{NBI}}\cdot\frac{2\nabla T_e}{T_e} \quad \text{eq.(2)}$$

For entirely beam heated plasmas $E_b=Q/\Gamma_{BNI}$ is the average beam energy (~90keV at JET). For typical $|\nabla T_e|/T_e \sim 2m^{-1}$ and T_e~3keV at mid radius, D would have to be ~10 times smaller than χ in order to explain a density gradient $|\nabla n_e|/n_e \sim 1m^{-1}$. For purely radio-frequency heated H-modes, as present in the dataset, only the Ware pinch or an anomalous pinch can contribute to density peaking. The contribution of the former can also be related to χ:

$$\left.\frac{\nabla n_e}{n_e}\right)_{Ware} = \frac{V_W}{D} = \frac{\chi}{D}\cdot\frac{V_W}{\chi}$$

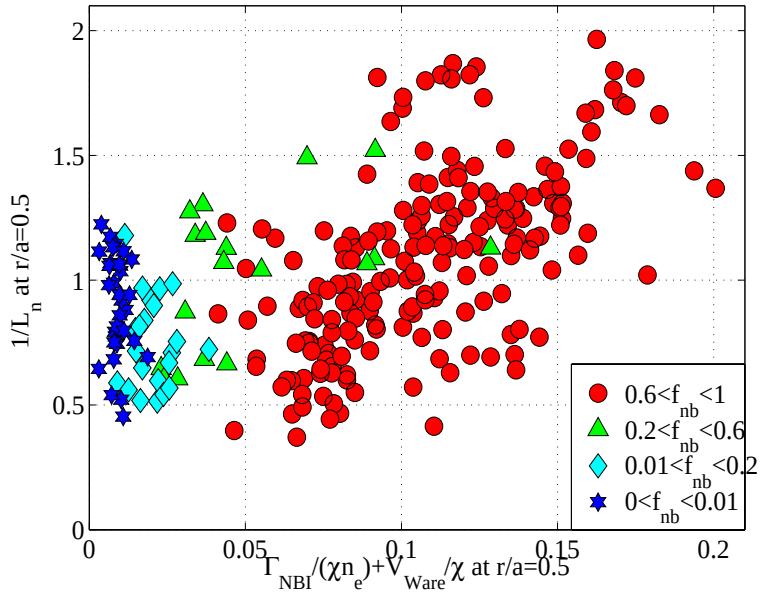

Fig. 2 Inverse density gradient length $|\nabla n_e|/n_e$ versus $\Gamma_{NBI}/(\chi n_e)+V_W/\chi$. Symbols refer to fraction of NBI heating.

On fig.2, we plot the experimental $|\nabla n_e|/n_e$ versus $\Gamma_{NBI}/(\chi n_e)+V_W/\chi$, evaluated at $r/a=0.5$. The figure presents the data presented in ref [7], supplemented by H-modes dominated by radio-frequency (RF) heating. The symbols refer to classes of $f_{nb}=Q_{NBI}/Q_{TOT}$. The contribution of the Ware pinch is comparable to, or larger than, the NBI contribution only for $P_{NBI}<2MW$ corresponding typically to $f_{nb}<0.2$. The variation of $\Gamma_{NBI}/(\chi n_e)$ for NBI dominated plasmas (red dots) stems not from changes in Γ_{NBI} (because$Q_{NBI}/\Gamma_{BNI}=E_b\approx$const), but from the range of ∇Te in the dataset. Considering only NBI dominated discharges, one could be misled to misinterpreteting the data

as a proof that NBI fuelling is the cause of density peaking. Considering also RF dominated discharges and Rf-only discharges (stars in fig.1), it becomes plain that there is no obvious correlation between $\nabla n_e/n_e$ and $\Gamma_{NBI}/(\chi n_e)+V_W/\chi$. In addition, the magnitude of D/χ required would have to be implausibly low, $\sim 10^{-2}$ for RF-only H-modes! We conclude that the combined beam fuelling and Ware pinch are unable to account for the observed density gradients, however beam fuelling may still be a significant contributor, depending on the real value of D/χ.

3. Dimensionless parameter interdependencies

Table 2: Correlation coefficients

	R/L_n	$n_{e0}/\langle n_e\rangle$	ν_{eff}	ν^*	N_G	$\Gamma/n_e\chi$	$\Gamma/n_e\chi+V_W/\chi$	V_W/χ	R/L_q	T_i/T_e	q_{95}	l_i	R/L_{Te}lid	β_N	ρ^*	R/L_{Ti}	R/L_{Te}ece
R/L_n		96	−65	−57	−63	61	57	−35	−33	29	28	−22	−21				
$n_{e0}/\langle n_e\rangle$	96		−71	−65	−70	53	50	−33	−21	26	25			−30			
ν_{eff}	−65	−71		94	85			52			−37			34	21		
ν^*	−57	−65	94		80			40						32			
N_G	−63	−70	85	80		−22		48	36		−30			42			−21
$\Gamma/n_e\chi$	61	53			−22		99		−47	31	44	−45					
$\Gamma/n_e\chi+V_W/\chi$	57	50				99			−43	30	38	−41					
V_W/χ	−35	−33	52	40	48				29	−20	−46	31		−21			−22
R/L_q	−33	−21			36	−47	−43	29		−30	−29	90		−27	−34		−35
T_i/T_e	29	26				31	30	−20	−30			−30	−38	34	25	−32	
q_{95}	28	25	−37		−30	44	38	−46	−29			−30	39		−36	26	57
l_i	−22					−45	−41	31	90	−30	−30			−58	−54	−22	−28
R/L_{Te}lid	−21									−38	39			−25	−36	33	48
β_N		−30	34	32	42			−21	−27	34		−58	−25		85		−30
ρ^*			21						−34	25	−36	−54	−36	85		20	−26
R/L_{Ti}										−32	26	−22	33		20		52
R/L_{Te}ece					−21			−22	−35		57	−28	48	−30	−26	52	

We wish to construct dimensionless scaling expressions for $R\nabla n_e/n_e$ and $n_{e0}/\langle n_e\rangle$, using both empirical scaling parameters and parameters inspired by theory. The latter, $R\nabla T_e/T_e$ $R\nabla T_i/T_i$ and $R\nabla q/q$ correspond to the thermodiffusive and curvature pinches respectively [8]. The effective collisionality $\nu_{eff}\approx 10^{-14} R Z_{eff} n_e/T_e^2$ governs drift wave stability and is predicted to influence the ratio of anomalous convection to particle diffusivity V/D [10]. β_N and ρ_e* are other key scaling parameters for drift wave driven transport and MHD stability. Instead of distinguishing between parameters for electrons and ions, we introduce T_i/T_e, which is theoretically expected to be related to the nature of the drift instability (ITG or TEM) and have a strong influence on particle convection [8]. We also include $R\Gamma_{NBI}/(\chi n_e)$, RV_W/χ and their sum in an attempt to account for the source and Ware pinch in the particle balance. The

Greenwald fraction $N_G=10^{14}\pi a^2\overline{n}_e I_p$ is not a 'canonical' dimensionless parameter, but has been included because it is a reference parameter for the ITER operation scenarios and displays a high degree of correlation with density peaking in H-mode.

Table 2 displays the cross correlation coefficients for $R\nabla n_e/n_e$, $n_{e0}/\langle n_e\rangle$ and the above named parameters. All local quantities are evaluated at or around (for gradients) r/a=0.5. The parameters with the highest cross correlation with $R\nabla n_e/n_e$ are ν_{eff}, N_G and $\Gamma_{NBI}/(\chi n_e)$, followed by T_i/T_e and $R\nabla q/q$. There is no indication for thermodiffusion, nor for dependencies on β_N and ρ_e*.

Figs 3 and 4 show the peaking factor versus ν_{eff} and N_G respectively. Fig.2 confirms an earlier observation of a dependence of density peaking on collisionality on AUG [10]. On fig.2 we see that H-modes with no or little NBI heating are on average somewhat less peaked that dominantly NBI heated discharges.

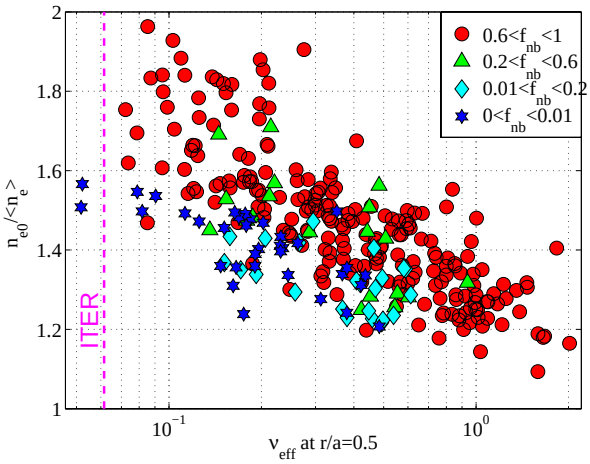

Fig. 3 Density peaking versus effective collisionality ν_{eff}. Symbols: fraction of NBI heating.

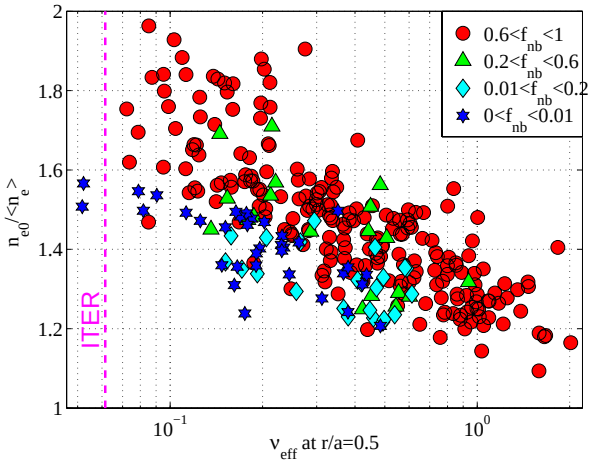

Fig. 4 Density peaking versus Greenwald number N_G. Symbols refer to ν_{eff}

4. Scaling with dimensionless parameters

In table 3 we construct a series of scaling expressions of the form $R\nabla n_e/n_e=c_0+\Sigma c_j p_j$, by including successively more parameters p_j, starting with those most strongly correlated with $R\nabla n_e/n_e$, until the corresponding coefficients c_j are too poorly defined for consideration and the standard deviation σ ceases to decrease. The intervals in he table correspond to 90% confidence. The last column provides the extrapolation to the ITER inductive scenario, assuming $\nu_{eff}=0.06$, $N_G=0.85$, $\Gamma=0$, $T_i/T_e=0.9$. As above, local parameters are taken at mid-radius. Used

Table 3: Scaling expressions for R/L_n

n_{fit}, n_e diagnostic	c_0	$\log\nu_{eff}$	N_G	$R\Gamma/n_e\chi$	T_i/T_e	l_i	σ_{fit}	ITER
1) SVDI	1.67±0.1	-1.35±0.2					0.52	3.3
2) SVDI	3.61±0.2		-2.58±0.4				0.53	1.42
3) SVDI	1.64±0.12			2.73±0.43			0.54	1.64
4) SVDI	2.48±0.5	-0.86±.34	-1.14±.66				0.51	2.56
5) SVDI	1.21±0.1	-1.18±.14		2.32±0.31			0.38	2.65
5) SVDI	2.86±0.2		2.12±0.3	2.22±0.34			0.42	1.06
6) SVDI	1.53±0.41	-0.99±.27	-0.43±.54	2.28±.31			0.38	2.37
7) SVDI	2.23±0.95	-1.27±.36	-0.39±.72		0.77±.33	-1.14±.72	0.31	3.1
8) SVDI	1.59±0.93	-1.03±.35	-0.59±0.68	1.21±0.54	0.60±0.32	-0.34±.76	0.29	2.57
9) SVDI	0.78±0.26	-1.28±.19		1.28±0.48	0.70±.31		0.29	2.97
10) SVDI	1.27±0.59	-1.01±.35	-0.62±.67	1.32±0.48	0.62±0.31		0.29	2.53
9') Lidar TS	*-0.14± .54*	*-1.36± .39*		*0.79± 0.98*	*0.83± 0.62*		*0.60*	*2.27*
10')Lidar TS	*0.84± 1.2*	*-0.82± .71*	*-1.23± 1.36*	*0.86± 0.97*	*0.68± 0.64*		*0.59*	*1.4*

Table 4: Scalings for $n_{e0}/\langle n_e\rangle$ and fusion power enhancement

c_0	$\log\nu_{eff}$	N_G	$R\Gamma/n_e\chi$	T_i/T_e	σ_{fit}	ITER $n_{e0}/\langle n_e\rangle$	ITER $n_{e95}/\langle n_e\rangle$	P_{DT}/P_{DT} flat fixed β and N_G	P_{DT}/P_{DT} flat fixed β and n_{e95}
1.22±0.15	-0.27±.09	-0.16±0.17	0.21±0.17	0.15±0.08	0.07	1.54	0.76	1.33	1.23
1.09±0.07	-0.34±.05		0.20±0.12	0.17±0.08	0.07	1.65	0.71	1.38	1.19

on their own, the three main parameters would provide conflicting predictions for ITER (fits no 1-3). However all combinations including ν_{eff} lead to the expectation of fairly peaked density profiles in ITER, with R/L_n typically in the range 2.4-3. The coefficient for the Ware pinch parameter RV_{Ware}/χ is too poorly defined for this parameter to be included in the scalings. Lumping RV_{Ware}/χ together with $R\Gamma/n_e\chi$ is practically equivalent to using $R\Gamma/n_e\chi$ alone. When N_G is included in a fit involving ν_{eff}, the corresponding coefficients become ill determined, suggesting that this parameter may not be an appropriate scaling parameter for density peaking. When local or global measures of magnetic shear (such as l_i in fits 7 & 8) are included, results depend on the presence of the particle flux term, their contribution becoming insignificant when the latter is included, as a result of correlations between these parameters.

The values of the coefficient for the particle flux parameter, $R\Gamma/n_e\chi$, can be interpreted as χ/D. We note that, when T_i/T_e is introduced as a fitting parameter, the value obtained for χ/D drops

from near 2.3 to 1.3. This can be understood from the twofold effect of NBI, which is to fuel, contributing to increasing the density gradients, and to increase the T_i/T_e ratio. An increase of T_i/T_e is expected to shift the balance of the unstable drift modes away from TEM's towards ITG's. According to drift wave turbulence theory [8], ITG's are characterised, in addition to a dominant inward anomalous curvature pinch, by inward thermodiffusion, whereas for TEM's, thermodiffusion is outward, leading to less peaking. The sign for the coefficient of T_i/T_e is consistent with this prediction, as is the value obtained for $\chi/D\approx1.3$, which is close to the theoretical value, 3/2 [8]. A value of $\chi/D\approx1.3$ is also within the range of χ/D_T obtained from experiments using trace amounts of tritium puffed into a large variety of JET discharges [12]

We offer scalings 9 and 10, which have the smallest σ, as the ones most probaby representative of the density peaking behaviour. Fits 1-10 are obtained from density profiles produced by inverting JET interferometer data by the SVD-I method [11], cross checked with a simple finite element method [13]. Profiles obtained from the JET LIDAR Thomson scattering system are more scattered due to statistical noise, but importantly, they are on average less peaked than those from interferometry, as seen in fits 9' and 10' in itallic in table 3. The discrepancy should be treated as a systematic uncertainty until resolved. Table 4 provides fits for the peaking factor using the parameters of the most succesful fits , 9 &10, in table 3.

5. Possible benefits and drawbacks for ITER

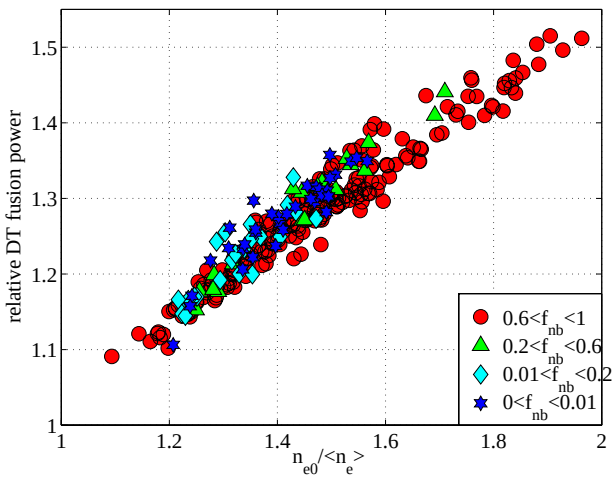

Fig. 5. Relative increase of fusion power with peaking factor for fixed N_G and β.

Before attempting to quantify the benefit of peaked density profiles for ITER fusion performance, we ascertain with the help of the correlation matrix (table 2) that temperature profile peaking is not correlated with density peaking, nor with any of the above scaling parameters for density scaling. Electron temperature profiles from LIDAR TS in JET have a large degree of variability, with no obvious correlation with operating conditions. For assessing the benefit in fusion performance, we therefore chose to select the electron temperature profile most similar to the ITER simulation in ref.[9], i.e.

T(0.95a)≈0.17T(0), scaled up to T(0)=18keV. The D-T fusion power is then calculated as $P_{DT} = 17.6 \times 10^6 e \int \langle \sigma v \rangle n_D n_T dV$ assuming first a flat density profile (as in [9]) for reference and then the whole range of density profiles observed experimentally normalised such as to have the same N_G. As the stored energy varies somewhat when the density profile is changed, the temperature profile is renormalised such as to conserve β and hence to remain within the restrictions of the operating scenario. In fig.5 we see that the ratio of P_{DT} from plasmas with peaked density profiles to that with the flat reference profile is almost entirely determined by the peaking factor. Projections for ITER (table 4) suggest an increase in fusion power of more than 30%. For the inductive scenario [9], which is heated by 80MW of alpha particle heating and 40MW of auxiliary heating, this means that most of the auxiliary heating can be replaced by the increased alpha power, leading to $Q_{fusion}>30$.

On the downside we have to consider that for fixed N_G and β, density peaking unavoidable-leads to a reduction of the pedestal density below the average density, by some 20-30% for the above ITER projections. This may affect divertor performance by making detachment more difficult. If however the density limit is linked to the pedestal density, rather than the line average density, a simple remedy is to raise the edge density to the target value with a corresponding temperature reduction to conserve β. In this case the effect of peaking is still beneficial, although somewhat less than at fixed average density (table 4).

Density peaking might provide a means to salvage fusion performance if the edge density limit drops to half of the expected value [14]. At constant β, fusion power with peaking expected for ITER in table 4, would still exceed the flat reference case by some 30%. However divertor operation at such a low density is questionable.

References

[1] G.T. HOANG et al, Phys. Rev. Lett. **90** (2003) 155002
[2]A. ZABOLOTSKY et al, Plasma Phys. Contr. Fusion **45** (2003) 735
[3]J. STOBER et al., Nuclear Fusion **41** (2001) 1535
[4]L. GARZOTTI et al, Nuclear Fusion **43** (2003) 1829
[5]M.VALOVIC et al, Plasma Phys. Contr.Fusion **46** (2004) 1877
[6]A. ZABOLOTSKY et al, submitted to Nuclear Fusion (2005)
[7] WEISEN H. et al, Nuclear Fusion **45** (2005) L1-L4
[8] X. GARBET et al (2004), Plasma Phys. Controll. Fusion **46** (2004) B577
[9]V. MUKHOVATOV et al, Plasma Phys. Contr. Fusion **45** (2003) A235

[10] C. ANGIONI et al, Phys. Rev. Lett. **90** (2003) 205003
[11] I. FURNO et al, Plasma Phys. Contr. Fusion **46** (2004)
[12] K.-D. ZASTROW et al, Plasma Phys. Controll. Fusion **46** (2004) B255
[13]A. ZABOLOTSKY, 'Particle transport in tokamak plasmas', PhD thesis, Ecole Polytechnique Fédérale de Lausanne EPFL, 2005
[14] K. BORRASS et al., Nuclear Fusion **44** (2004) 752